Published in final edited form as:
Ultrastruct Pathol. 2014 August ; 38(4): 248–255. doi:10.3109/01913123.2013.815081.

"A New Tool Improves Diagnostic Test Performance for Transmission EM Evaluation of Axonemal Dynein Arms"

W. Keith Funkhouser III,
Department of Biostatistics, University of North Carolina at Chapel Hill

Marc Niethammer, PhD,
Department of Computer Science, University of North Carolina at Chapel Hill

Johnny L. Carson, PhD,
Departments of Pediatrics and Cell and Development Biology, The Center for Environmental Medicine, Asthma and Lung Biology, University of North Carolina at Chapel Hill

Kimberlie A. Burns, BS, HTL,
Department of Pulmonary Medicine, University of North Carolina at Chapel Hill

Michael R. Knowles, MD,
Pulmonary/Cystic Fibrosis Research and Treatment Center, University of North Carolina at Chapel Hill

Margaret W. Leigh, MD,
Pulmonary/Cystic Fibrosis Research and Treatment Center, University of North Carolina at Chapel Hill

Maimoona A. Zariwala, PhD, and
Department of Pathology and Laboratory Medicine, University of North Carolina at Chapel Hill

William K. Funkhouser Jr., MD, PhD
Department of Pathology and Laboratory Medicine, University of North Carolina at Chapel Hill

Abstract

Diagnosis of primary ciliary dyskinesia (PCD) by identification of dynein arm loss in transmission electron microscopy (TEM) images can be confounded by high background noise due to random electron-dense material within the ciliary matrix, leading to diagnostic uncertainty even for experienced morphologists. We developed a novel image analysis tool to average the axonemal peripheral microtubular doublets, thereby increasing microtubular signal and reducing random background noise. In a randomized, double-blinded study that compared two experienced morphologists and three different diagnostic approaches, we found that use of this tool led to improvement in diagnostic TEM test performance.

Address correspondence to: **William K. Funkhouser, MD PhD**, CB # 7525, Department of Pathology and Laboratory Medicine, University of North Carolina at Chapel Hill, Chapel Hill, NC 27599-7525, USA, Bill_Funkhouser@med.unc.edu.

Declaration of interest: The authors report no conflicts of interest. The authors alone are responsible for the content and writing of the paper. No financial support was received for execution of this project.

Introduction

Cilia are evolutionarily-conserved common cellular processes that have either sensory ("primary" cilia) or motor ("motile" cilia) functions, and whose loss-of-function defects result in disease phenotypes [1], including the ciliopathies [2] and primary ciliary dyskinesia [3]. Sensory and motile cilia share a characteristic axonemal architecture of 9 peripherally located microtubular pairs [1]. Motile cilia have dynein arm multimers that hydrolyze ATP [4] to generate mechanical torque [5] by forced sliding of adjacent peripheral microtubular pairs [6]. Motile cilia without two-microtubule central complexes ("9+0" architecture) move in a rotatory fashion, and are responsible for a fluid current at the embryonic node that determines sidedness in the developing embryo [7]. In contrast, motile cilia with two-microtubule central complexes ("9+2" architecture) have an effective stroke in a single plane, such that synchronous (per cell) and metachronous (per surface) beating allows coordinated movement of surface fluid [8, 9].

Primary ciliary dyskinesia (PCD) (primary here implies congenital, rather than acquired, and not involvement of primary cilia) is a human disease (OMIM 244400) that affects the structure and/or function of motile cilia and flagella [1, 9], leading to early onset sino-pulmonary infections, bronchiectasis, and male sterility [9-11]. Although early diagnosis and management benefit these patients [12, 13], there is substantial delay in diagnosis [14]. The originally-described patients with immotile sperm flagella and absent muco-ciliary transport were found to have missing dynein arms [15-17]. Larger series subsequently found ultrastructural loss or truncation of dynein arms in 80-90%, and central complex defects in 15-20%, of patients with clinical PCD and specific ultrastructural defects [18, 19]. A larger series also found that 5% of cases showed either acquired ultrastructural changes related to mucosal damage, or equivocal ultrastructural changes related to low signal:noise [19]. Although initial studies assumed that all PCD cases had specific axonemal ultrastructural defects, subsequent studies have found DNAH11-mutant patients with clinical PCD, but without ultrastructural defects [20, 21]. Three different clinical series of a total of 577 PCD cases found normal ultrastructure in 18% [22], 29% [19], and 30% [21] of the PCD cases. If 70% of true PCD cases show a ciliary ultrastructural abnormality, and if 90% of ciliary ultrastrucutural defects in PCD involve the dynein arms, then roughly 60-65% of actual PCD cases (TEM screening sensitivity) will show specific defects of the axonemal dynein arms. Because of this frequency of dynein arm dysmorphology in PCD, and because of the specificity of this finding, it is important for diagnostic morphologists to optimize visualization of dynein arm ultrastructure.

Optimization of glutaraldehyde/paraformaldehyde fixation with addition of tannic acid, as well as optimization of staining with uranyl acetate, allows improved signal-to-noise of TEM images [23]. However, despite optimal protocols for tissue sampling and processing, images can still show high background noise from random electron-dense material in the ciliary matrix [24]. This high background leads to low signal-to-noise ratios, confounding interpretation of axonemal ultrastructure. It would thus be desirable to develop methods that accentuate relevant ciliary structures and reduce ciliary matrix background noise. This has been previously accomplished using manual registration of peripheral microtubular pairs [23-25] and using affine transformations based on the centers of peripheral microtubular

pairs [26] to produce a composite, low-noise image. However, each of these methods suffers from various drawbacks, including dependence on circular symmetry of the axoneme [24, 26], lack of automation [23, 25, 26], and dependence on homogeneity of peripheral microtubular pair shape [26]. We have developed a semi-automated image analysis tool that processes high-noise digital TEMs and outputs low-noise averaged images of the peripheral microtubular pairs. In a randomized, double-blind experiment, we found that use of this image-averaging tool led to increases in TEM diagnostic test performance for each of two experienced morphologists.

Materials and Methods

Tool design

Two of us (KF, MN) designed a tool in the MATLAB environment that allows the user to successively process digital images of ciliary axonemes. Analysis begins with user selection of upper left and lower right bounds of a given axoneme. This section is then extracted and processed further by user selection of individual peripheral microtubular pairs, which are themselves extracted. The first peripheral microtubular pair is then used as a template to which the following peripheral microtubular pairs are registered. Registration is performed using an affine transformation that allows for rotation and scaling. The sum of square differences (SSD) between the two peripheral microtubular pairs is minimized. Each subsequent peripheral microtubular pair is registered in this way and averaged in.

The workflow, shown in Figure 1, consists of 1) selection of the 10 “highest-quality” axonemes (based on a qualitative assessment of plane of section and signal:noise ratio) and 2) selection of the peripheral microtubular pairs from these axonemes. Successive registration is then performed to produce the low-noise output. The output is in two groups: 1) “per-axoneme” averaged images (1 image per ciliary axoneme, each image the average of 9 peripheral microtubular pairs, so 10 images), and 2) a single “all-axonemes” averaged image (the average of all 90 peripheral microtubular pairs in the 10 axonemes) (Figure 2).

Biopsy Sources and Tissue Processing

Nasal mucosal scrape cytology preparations were obtained from consented adults and children seen by pulmonologists and clinical scientists at UNC following referral for formal evaluation for cystic fibrosis (CF) and PCD. Biopsy tissues were subjected to primary fixation by immersion in buffered 2% glutaraldehyde/2% paraformaldehyde supplemented with 0.5% tannic acid for 5 days to 3 months at 4°C, post-fixed for 1 hr. at 4°C in 1% osmium tetroxide, dehyrated through graded ethanols, and embedded in epoxy resin. Although ours is a well-recognized center of PCD research, PCD nevertheless is a rare disease, and the patient population from which appropriate specimens are derived is relatively small. Thus, it has been our practice to store specimens until sufficient numbers have been received, in order to facilitate processing and to achieve optimal quality control. We have previously shown excellent ultrastructural preservation of nasal mucosal biopsies that required extended fixation [27]. Ultrathin (60-90 nm) sections were cut and post-stained in uranyl acetate and lead citrate. Stained sections were viewed and photographed in a Zeiss EM900 transmission electron microscope at a standard accelerating voltage of 50 kV.

Experimental design

A total of 26 cases were selected from the UNC Cystic Fibrosis Center TEM library by one of us (ML). Each case was assigned an overall best clinical diagnosis by one of us (ML) of PCD (n=19) or not affected/normal (n=7), based on all available data from clinical presentation, family history, radiographs, TEM, ciliary videomicroscopy, nasal nitric oxide (NO), and genetic sequencing. A summary of the cases is given in Table 1. The set of TEM images from each case was scanned by one of us (KF) on an Epson Expression 10000XL at 400dpi in 8 bit grayscale Tagged Image Format (TIFF). The 10 “highest quality” ciliary axonemes (based on a qualitative assessment of plane of section and signal:noise ratio) per case were selected, processed using the tool, and their output saved for each case. Thus, each case was represented 3 ways, i.e. as 1) a set of raw TEM digital images per case, 2) a set of ten per-axoneme averaged images per case, and 3) one all-axonemes averaged image per case.

These three sets of diagnostic images were then evaluated by two experienced TEM morphologists (JLC, WF). For the first method, the morphologists were given the digital scans of all of the raw TEM images for a given case; this was considered to model the current approach to TEM diagnosis. For the second method, the morphologists were given the 10 per-axoneme averaged images. For the third method, the morphologists were given the single all-axonemes averaged image. The case order was randomized for each of the two morphologists, and for each method. Corresponding image files were assembled within a folder structure in such a way that they could be browsed. A spreadsheet was prepared so that the morphologists’ evaluations could be recorded. Each case was scored for the presence or absence of each of the dynein arms. No teaching set was used prior to the experiment. Each morphologist used his own diagnostic criteria regarding whether dynein arm truncation was sufficient to diagnose a dynein arm defect.

Analysis

Accuracy, sensitivity, specificity, negative predictive value (NPV), and positive predictive value (PPV) were calculated for inner dynein arms (IDA), outer dynein arms (ODA), and both combined dynein arms for the 26 cases, and for each observer. Inter-rater reliability was calculated between morphologists using Cohen’s kappa [28] for each method for all cases (n=26). All data analyses were performed using SPSS version 9.0 (SPSS, Inc., Chicago IL). Inter-rater reliability results are presented in the form kappa ± asymptotic standard error (SE).

Results

TEM Diagnostic Inter-Rater Reliability

For the entire set of 26 cases, inter-rater reliability was calculated between morphologists for each method (Figure 3). For raw TEM diagnosis, overall kappa including both IDA and ODA interpretations was 0.762 ± 0.100. For diagnosis using multiple per-axoneme averaged images, the overall kappa was 0.952 ± 0.047. For diagnosis using a single all-axonemes averaged image, the overall kappa was 0.867 ± 0.074. Kappa values for just the IDA or the ODA are also shown in Figure 3.

TEM Diagnostic Test Performance

Test performance was determined for the three different tests by comparing observed and expected dynein arm status for each of the 26 cases. For Observer #1, diagnoses of dynein arm defects showed increasing sensitivity, specificity, PPV, NPV, and accuracy with use of tool output (Table 2). When using raw TEM, Observer #1 would have generated 2 false positive PCD diagnoses (calling dynein-arm-defect PCD when the dynein arms were normal), and would have made 3 false negative PCD diagnoses (calling normal when one of the dynein arms was defective). When using per-axoneme averages, Observer #1 would have made 1 false positive PCD diagnosis, and would have made no false negative PCD diagnoses. When using the single all-axonemes average, Observer #1 would have made 1 false positive PCD diagnosis, and would have made no false negative PCD diagnoses.

For Observer #2, test performance was high with all methods, with minimal room for improvement over conventional raw TEM analysis. PPV improved with use of tool output (Table 2). When using raw TEM, Observer #2 would have made 1 false positive diagnosis (calling dynein-arm-defect PCD when the dynein arms were normal), and no false negative diagnoses. When using per-axoneme averages, Observer #2 would have made no false positive or false negative PCD diagnoses. When using the single all-axonemes average, Observer #2 would have made 1 false positive PCD diagnosis, and would have made no false negative PCD diagnoses.

For the 7 unaffected individuals, no inner dynein arm loss was expected, but inner arm loss was observed in 4 of 42 diagnoses. Three of these four discrepant diagnoses were made using the raw TEM images, one was made using the multiple per-axoneme averaged images, and none were made using the single all-axonemes averaged images. These data suggest improved imaging of the inner dynein arms when using the image analysis tool. In these 7 unaffected individuals, no outer dynein arm loss was expected, and no outer dynein arm loss was observed using any of the three methods.

For the 10 PCD cases with inner dynein arm loss, inner dynein arms were called present in 5 of 60 diagnoses. Two of these five discrepant diagnoses were made using the raw TEM images, two were made using the multiple per-axoneme averaged images, and one was made using the single all-axonemes averaged images.

For the 5 PCD cases with outer dynein arm loss, outer dynein arms were called present in 2 of 30 diagnoses. Both of these discrepant diagnoses were made using the raw TEM images.

Genetic Testing

Subsequent to design of this study, genetic studies have confirmed the diagnosis of PCD by identification of biallelic loss of function mutations in 10 cases (Table 1). For the 6 cases with mutations in genes associated with dynein arm defects (*DNAH5* [29, 30], *DNAAF1* [31], *CCDC40* [32]), all had identified dynein arm defects. For the 4 cases with mutations in genes associated with normal dynein arms (*RSPH4A* [33] and *DNAH11* [21]), no dynein arm defects were identified by our analyses. Therefore, our interpretation of dynein defects is congruent with these genetic studies.

Discussion

Specific ciliary axonemal ultrastructural defects are expected in about 70% of PCD cases by TEM [19, 21, 22], and about 90% of these will involve dynein arm defects [18, 19]. TEM testing is incorporated into a global clinical workup that includes family history, sino-pulmonary disease history, radiography screening for bronchiectasis, nasal nitric oxide concentration, ciliary beat frequency/kinetics, and germline gene mutation testing. For the 60-65% of cases in which the TEM finding of dynein arm loss can support a diagnosis of PCD, TEM background noise can confound ultrastructural diagnosis, leading to diagnostic uncertainly even for experienced morphologists. Our tool improves the signal strength of the peripheral microtubular pair, and reduces the noise from random ciliary matrix electron-dense material around the inner and outer dynein arms. We tested the hypothesis that axonemal ultrastructural diagnosis using our tool's outputs would improve diagnostic test performance when compared with conventional raw TEM analysis.

Our tool is based on the concept that virtual stacking of predictably-sized structures will amplify the signal of the structure, and will reduce the random background noise during the averaging process. This has been shown to work for structures with rotational symmetry using manual darkroom-based [34] and computer-based methods [24, 26]. It has also been shown to work for isolated images of peripheral microtubular pairs using manual alignment [25]. The first novel contribution of this study is the use of a computer to calculate optimal (least-squares) alignment for the stacked microtubular pairs, requiring no assumptions about axonemal symmetry, requiring minimal assumptions about peripheral microtubular pair shape, and allowing virtual stacking of more than 9 microtubular pairs in a single averaged image.

The second novel contribution of this study is the quantification of test performance for TEM used to diagnose dynein arm loss in ciliary axonemes. Previous studies alluded to improved diagnosis due to improved visualization. We tested the hypothesis that axonemal ultrastructural diagnosis using our tool's outputs would improve diagnostic test performance when compared with conventional raw TEM analysis. We were able to test this hypothesis because of the availability of thoroughly worked-up cases through the UNC Pulmonary/CF Research and Treatment Center. We found that inter-rater reliability and TEM diagnostic test performance for detection of dynein arm defects improved when observers used averaged images. The best test for detection of dynein arm defects in this study was the set of 10 peraxoneme averaged images, which showed high inter-rater reliability (kappa=0.95), sensitivity (0.93), specificity (≥0.97), accuracy (≥0.96), PPV (≥0.93), and NPV (0.97).

Further studies will aim to correlate the degree of inner and outer dynein arm truncation with the probability of axonemal physiologic dysfunction, alteration of nasal nitric oxide production, and germline genetic mutation. These demonstrated improvements in TEM test performance will hopefully contribute, along with improvements in ciliary video imaging, nasal nitric oxide testing, and gene mutation testing, to earlier diagnosis and management of patients and their at-risk sibs.

Acknowledgments

This research was supported in part by NIH Grants 5-P41-EB002025, 5R01HL071798, and 5U54HL096458.

References

1. Afzelius BA. Cilia-related diseases. J Pathol. 2004; 204(4):470–7. [PubMed: 15495266]
2. Hildebrandt F, Benzing T, Katsanis N. Ciliopathies. New England Journal of Medicine. 2011; 364(16):1533–1543. [PubMed: 21506742]
3. Zariwala MA, Knowles MR, Omran H. Genetic defects in ciliary structure and function. Annu. Rev. Physiol. 2007; 69:423–450. [PubMed: 17059358]
4. Pfister KK, Fay RB, Witman GB. Purification and polypeptide composition of dynein ATPases from Chlamydomonas flagella. Cell Motil. 1982; 2(6):525–47. [PubMed: 6220806]
5. Yoneda M. Force exerted by a single cilium of mytilus edulis. Experimental Biology. 1962; 39:307–318.
6. Satir P. STUDIES ON CILIA: II. Examination of the Distal Region of the Ciliary Shaft and the Role of the Filaments in Motility. J Cell Biol. 1965; 26(3):805–34. [PubMed: 19866682]
7. Nonaka S, Yanaka Y, Okada Y, et al. Randomization of left-right asymmetry due to loss of nodal cilia generating leftward flow of extraembryonic fluid in mice lacking KIF3B motor protein. Cell. 1998; 95(6):829–37. [PubMed: 9865700]
8. Aiello E, Sleigh MA. The metachronal wave of lateral cilia of Mytilus edulis. J Cell Biol. 1972; 54(3):493–506. [PubMed: 5044757]
9. Palmblad J, Mossberg B, Afzelius BA. Ultrastructural, cellular, and clinical features of the immotile-cilia syndrome. Annu Rev Med. 1984; 35:481–92. [PubMed: 6372667]
10. Noone PG, Leigh MW, Sannuti A, et al. Primary Ciliary Dyskinesia: Diagnostic and Phenotypic Features. American Journal of Respiratory and Critical Care Medicine. 2004; 169:459–67. [PubMed: 14656747]
11. Leigh MW, Pittman JE, Carson JL, et al. Clinical and genetic aspects of primary ciliary dyskinesia/Kartagener syndrome. Genetics in Medicine. 2009; 11(7):473–487. [PubMed: 19606528]
12. Ellerman A, Bisgaard H. Longitudinal study of lung function in a cohort of primary ciliary dyskinesia. Eur Respir J. 1997; 10(10):2376–9. [PubMed: 9387968]
13. Coren ME, Meeks M, Morrison I, et al. Primary ciliary dyskinesia: age at diagnosis and symptom history. Acta Paediatr. 2002; 91(6):667–9. [PubMed: 12162599]
14. Leigh MW, O'Callaghan C, Knowles MR. The challenges of diagnosing primary ciliary dyskinesia. Proceedings of the American Thoracic Society. 2011; 8(5):434–437. [PubMed: 21926395]
15. Afzelius BA, Eliasson R, Jonsen O, et al. Lack of dynein arms in immotile human spermatozoa. J Cell Biol. 1975; 66(2):225–32. [PubMed: 1141381]
16. Camner P, Mossberg B, Afzelius BA. Evidence of congenitally nonfunctioning cilia in the tracheobronchial tract in two subjects. Am Rev Respir Dis. 1975; 112(6):807–9. [PubMed: 1081860]
17. Pedersen H, Mygind N. Absence of axonemal arms in nasal mucosa cilia in Kartagener's syndrome. Nature. 1976; 262(5568):494–5. [PubMed: 1085417]
18. Sturgess JM, Thompson MW, Czegledy-Nagy E, et al. Genetic aspects of immotile cilia syndrome. Am J Med Genet. 1986; 25(1):149–60. [PubMed: 3492145]
19. Papon JF, Coste A, Roudot-Thoraval F, et al. A 20-year experience of electron microscopy in the diagnosis of primary ciliary dyskinesia. Eur Respir J. 2010; 35(5):1057–63. [PubMed: 19840971]
20. Bartoloni L, Blouin J-L, Pan Y, et al. Mutations in the DNAH11 (axonemal heavy chain dynein type 11) gene cause one form of situs inversus totalis and most likely primary ciliary dyskinesia. Proc Natl Acad Sci U S A. 2002; 99(16):10282–6. [PubMed: 12142464]
21. Knowles MR, Leigh MW, Carson JL, et al. Mutations of DNAH11 in patients with primary ciliary dyskinesia with normal ciliary ultrastructure. Thorax. 2012; 67:433–41. [PubMed: 22184204]

22. Jorissen M, Willems T, Van der Schueren B. Ciliary function analysis for the diagnosis of primary ciliary dyskinesia: advantages of ciliogenesis in culture. Acta Otolaryngol. 2000; 120(2):291–5. [PubMed: 11603792]

23. Afzelius BA, Dallai R, Lanzavecchia S, et al. Flagellar structure in normal human spermatozoa and in spermatozoa that lack dynein arms. Tissue Cell. 1995; 27(3):241–7. [PubMed: 7645004]

24. Carson JL, Hu SCS, Collier AM. Computer-assisted analysis of radial symmetry in human airway epithelial cilia: assessment of congenital ciliary defects in primary ciliary dyskinesia. Ultrastructural Pathology. 2000; 24(3):169–174. [PubMed: 10914428]

25. Kamiya R, Kurimoto E, Muto E. Two types of Chlamydomonas flagellar mutants missing different components of inner-arm dynein. J Cell Biol. 1991; 112(3):441–7. [PubMed: 1825085]

26. Escudier E, et al. Computer-assisted analysis helps detect inner dynein arm abnormalities. Am J Respir Crit Care Med. 2002; 166(9):1257–62. [PubMed: 12403696]

27. Carson JL, Collier AM, Hu S.-c.S. Acquired ciliary defects in nasal epithelium of children with acute viral upper respiratory infections. The New England journal of medicine. 1985; 312:463–8. [PubMed: 3969108]

28. Cohen J. A coefficient of agreement for nominal scales. Educational and psychological measurement. 1960; 20(1):37–46.

29. Hornef N, Olbrich H, Horvath J, et al. DNAH5 mutations are a common cause of primary ciliary dyskinesia with outer dynein arm defects. American journal of respiratory and critical care medicine. 2006; 174(2):120–126. [PubMed: 16627867]

30. Ferkol TF, P.E. Lie H, et al. Primary ciliary dyskinesia-causing DNAH5 mutations in Amish communities. J Pediatr. 2013; 163:309–11. in press 2013.

31. Loges NT, Olbrich H, Becker-Heck A, et al. Deletions and Point Mutations of LRRC50 Cause Primary Ciliary Dyskinesia Due to Dynein Arm Defects. The American Journal of Human Genetics. 2009; 85(6):883–889.

32. Antony D, Becker-Heck A, Zariwala MA, et al. Mutations in CCDC39 and CCDC40 are the major cause of primary ciliary dyskinesia with axonemal disorganisation and absent inner dynein arms. Hum Mutat. 2013; 34:462–72. [PubMed: 23255504]

33. Daniels, ML.; Leigh, MW.; Davis, SD., et al. The American Society of Human Genetics. San Francisco, CA, USA: 2012. Founder mutation in RSPH4A identified in patients of Hispanic descent with primary ciliary dyskinesia.

34. Markham R, Frey S, Hills GJ. Methods for the Enhancement of Image Detail and Accentuation of Structure in Electron Microscopy. Virology. 1963; 20:88–102.

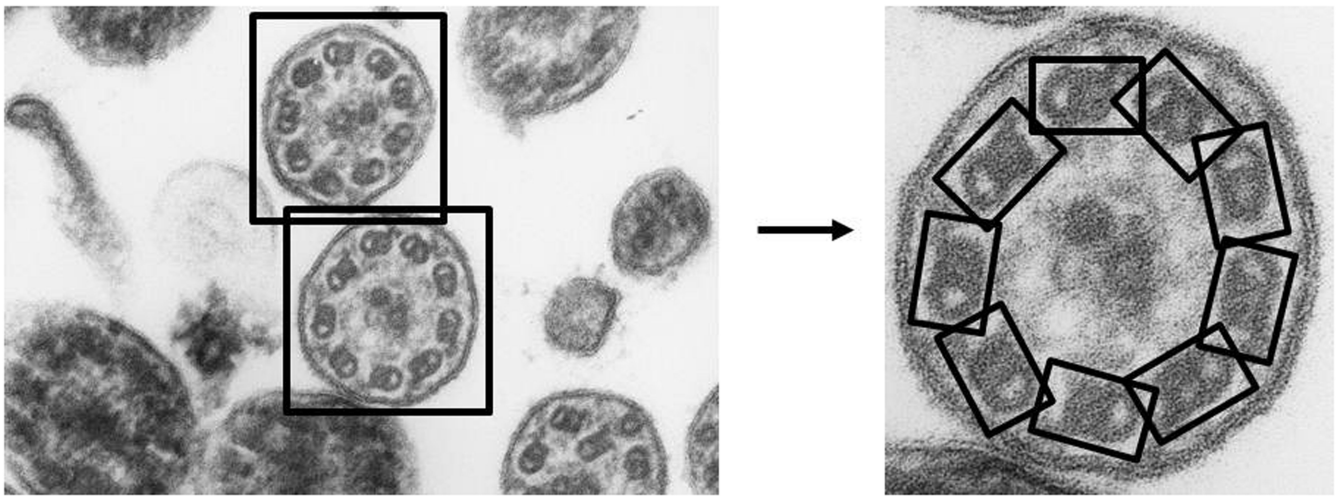

Figure 1.

TEM images are processed by the tool in two steps. In the first step, axonemes are segmented from the original, followed by selection of microtubular doublets to be averaged.

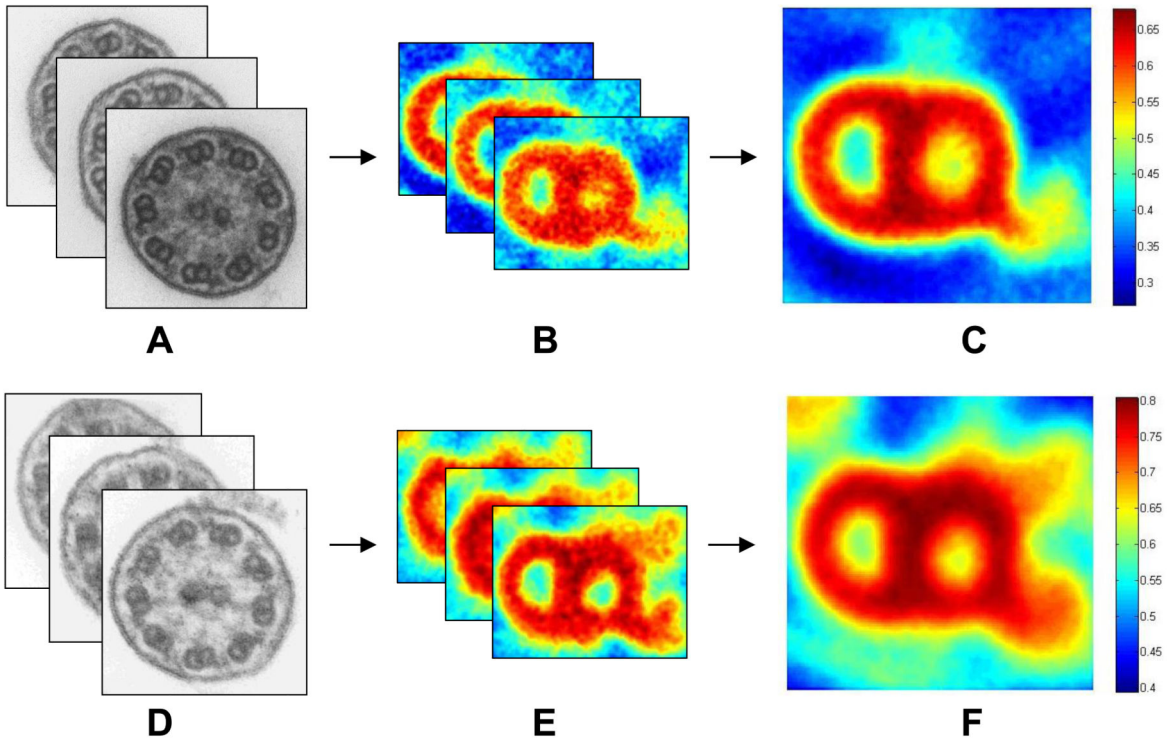

Figure 2.

After selection and processing of ten axonemes (A,D), the tool generates output in two forms: a set of per-axoneme averages (B,E) and a single average (C,F). Averages (B,C,E,F) are oriented so that the lower dynein arm represents the outer dynein arm. Images A-C illustrate the tool's ability to increase signal:noise in case 12, which is missing the inner dynein arm. Images D-F illustrate the tool's ability to better visualize the inner dynein arm in case 3, which has normal ultrastructure.

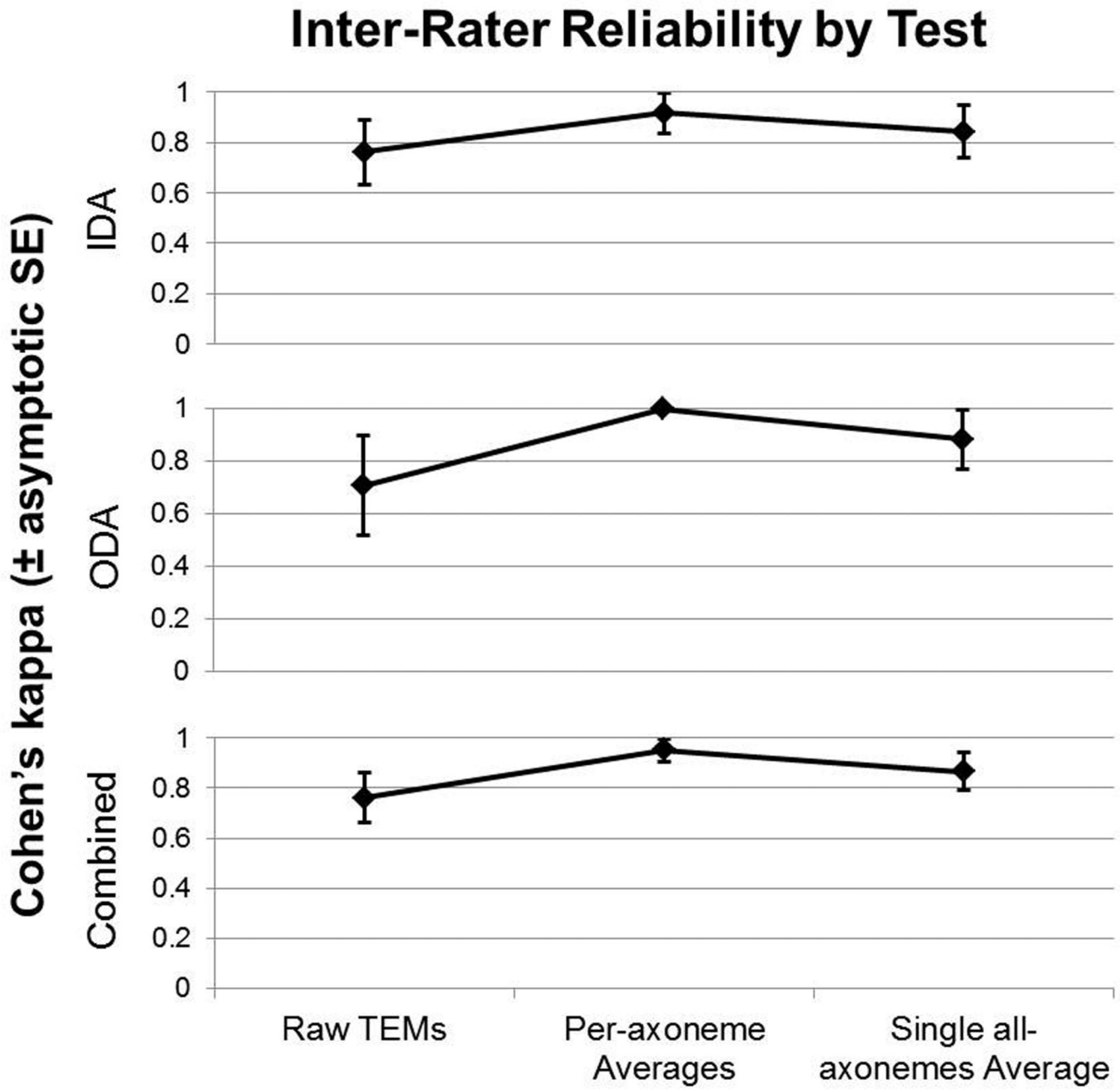

Figure 3.

Results of inter-rater reliability analysis for the two morphologists, using conventional raw TEM, per-axoneme averaged images, and a single all-axonemes averaged image. Cohen's kappa along with asymptotic standard error bars are shown for each method. The upper panel shows kappa for evaluation of IDA, the middle panel for evaluation of ODA, and the lower panel for the combination of both IDA and ODA.

Table 1

Patient data and observational data

ID	Relationship to patient	Best Clinical Diagnosis	PCD Gene	Type of Biallelic Mutations	Expected TEM Diagnosis of Dynein Arms	Raw TEM Images[a]				Per-Axoneme Averages[b]				Single All-axonemes Average[c]			
						Obs. 1		Obs. 2		Obs. 1		Obs. 2		Obs. 1		Obs. 2	
						IDA	ODA	IDA	ODA	IDA	ODA	IDA	ODA	IDA	ODA	IDA	ODA
1	parent	Unaff.			Normal												
2	patient	PCD			ODA, IDA def.	____	Def.	Def.	Def.	____	Def.	____	Def.	____	Def.	Def.	Def.
3	parent	Unaff.			Normal												
4	unaffected sib	Unaff.			Normal												
5	parent	Unaff.			Normal	Def.											
6	parent	Unaff.			Normal					Def.							
7	patient	PCD	DNAAF1 (LRRC50)* [31]	nonsense/deletion	ODA, IDA def.	Def.	Def.	Def.	Def.	Def.	Def.	Def.	Def.	Def.	Def.	Def.	Def.
8	unaffected sib	Unaff.			Normal												
9	unaffected sib	Unaff.			Normal	Def.		Def.									
10	patient	PCD&			IDA def.	Def.		Def.		Def.		Def.		Def.	Def.	Def.	
11	patient	PCD	DNAH11* [34]	nonsense/nonsense	Normal												
12	patient	PCD	CCDC40* [32]	nonsense/frameshift	IDA def.	Def.		Def.		Def.		Def.		Def.		Def.	
13	patient	PCD	RSPH4A* [33]	homozygous splice-site	Normal												
14	patient	PCD	DNAH5* [29,30]	homozygous nonsense	ODA def.		Def.		Def.		Def.		Def.		Def.		Def.
15	patient	PCD	CCDC40* [32]	homozygous frameshift	IDA def.	Def.		Def.		Def.		Def.		Def.		Def.	
16	patient	PCD			IDA def.	____		Def.		Def.		Def.		Def.		Def.	
17	patient	PCD	DNAH5 [29,30]		Normal									Def.		Def.	
18	patient	PCD		frameshift/splice-site	ODA def.		____		Def.		Def.		Def.		Def.	Def.	Def.
19	patient	PCD			ODA def.		____		Def.		Def.		Def.		Def.		Def.
20	patient	PCD			IDA def.	Def.		Def.		Def.		Def.		Def.		Def.	
21	patient	PCD			Normal												
22	patient	PCD			IDA def.	Def.		Def.		Def.		Def.		Def.		Def.	
23	patient	PCD	CCDC40* [32]	homozygous frameshift	IDA def.	Def.		Def.		Def.		Def.		Def.		Def.	

ID	Relationship to patient	Best Clinical Diagnosis	PCD Gene	Type of Biallelic Mutations	Expected TEM Diagnosis of Dynein Arms	Raw TEM Images[a]				Per-Axoneme Averages[b]				Single All-axonemes Average[c]			
						Obs. 1		Obs. 2		Obs. 1		Obs. 2		Obs. 1		Obs. 2	
						IDA	ODA	IDA	ODA	IDA	ODA	IDA	ODA	IDA	ODA	IDA	ODA
24	patient	PCD			IDA def.	Def.		Def.		Def.		Def.		Def.		Def.	
25	patient patient	PCD	RSPH4A* [33]	frameshift/splice-site	Normal												
26	patient	PCD	RSPH4A* [33]	homozygous splice-site	Normal												

Def. = Defective or absent.

‘____’ = error cf. expected

&Same patient as number 16.

[a]Errors that would affect diagnosis were found in 6 of 26 patients (52 diagnoses, 12%) (3 F(+), 3 F(−)).

[b]Errors that would affect diagnosis were found in 1 of 26 patients (52 diagnoses, 2%) (F(+)).

[c]Errors that would affect diagnosis were found in 2 of 26 patients (52 diagnoses, 4%) (F(+)).

*Genetic data included in publication referenced

Table 2

Test Performance

	Raw TEMs			Per-axoneme Averages			Single All-Axonemes Average		
Obs 1	**IDA**	**ODA**	**Combined**	**IDA**	**ODA**	**Combined**	**IDA**	**ODA**	**Combined**
PPV	0.80	1.00	0.85	0.90	1.00	0.93	0.90	0.83	0.88
NPV	0.88	0.91	0.90	0.94	1.00	0.97	0.94	1.00	0.97
Sensitivity	0.80	0.60	0.73	0.90	1.00	0.93	0.90	1.00	0.93
Specificity	0.88	1.00	0.95	0.94	1.00	0.97	0.94	0.95	0.95
Accuracy	0.85	0.92	0.88	0.92	1.00	0.96	0.92	0.96	0.94
Obs 2									
PPV	0.91	1.00	0.94	1.00	1.00	1.00	0.83	1.00	0.88
NPV	1.00	1.00	1.00	0.94	1.00	0.97	1.00	1.00	1.00
Sensitivity	1.00	1.00	1.00	0.90	1.00	0.93	1.00	1.00	1.00
Specificity	0.94	1.00	0.97	1.00	1.00	1.00	0.88	1.00	0.95
Accuracy	0.96	1.00	0.98	0.96	1.00	0.98	0.92	1.00	0.96